https://doi.org/10.5194/acp-2020-1273
Preprint. Discussion started: 8 January 2021

Atmospheric Chemistry and Physics Discussions

Lidar vertical observation network and data assimilation reveal key processes driving the 3-D dynamic evolution of $PM_{2.5}$ concentrations over the North China Plain

Yan Xiang[1], Tianshu Zhang[2, 1], Chaoqun Ma[3], Lihui Lv[1], Jianguo Liu[2], Wenqing Liu[2, 1], and Yafang Cheng[3]

[1]Institutes of Physical Science and Information Technology, Anhui University, Hefei 230601, China
[2]Key Laboratory of Environmental Optics and Technology, Anhui Institute of Optics and Fine Mechanics, Chinese Academy of Sciences, Hefei 230031, China
[3]Minerva Research Group, Max Planck Institute for Chemistry, Mainz, Germany

Correspondence: Yan Xiang (yxiang@ahu.edu.cn) and Yafang Cheng (yafang.cheng@mpic.de)

Abstract: China has made great efforts to monitor and control air pollution in the past decade. Comprehensive characterization and understanding of pollutants in three-dimension (3-D) are, however, still lacking. Here, we used data from an observation network consisting of 13 aerosol lidars and more than 1000 ground observation stations, combined with a data assimilation technique, to conduct a comprehensive analysis of an extreme heavy aerosol pollution (HAP) over the North China Plain (NCP) from November–December 2017. During the studied period, the maximum hourly mass concentration of surface $PM_{2.5}$ reached ~390 $\mu g \cdot m^{-3}$. After assimilation, the correlation between model results and the independent observation sub-dataset was ~50% higher than the that without the assimilation, and the root mean square error was reduced by ~40%. From pollution development to dissipation, we divided the HAP in the NCP (especially in Beijing) into four phases—an early phase (EP), a transport phase (TP), an accumulation phase (AP), and a removal phase (RP). We then analyzed the evolutionary characteristics of $PM_{2.5}$ concentration during different phases on the surface and in 3-D space. We found that the particles were mainly transported from south to north at a height of 1-2 km (during EP and RP) and near the surface (during TP and AP). The amounts of $PM_{2.5}$ advected into Beijing with the maximum transport flux intensity (TFI) were through the pathways in the relative order of the southwest > southeast > east pathways. The dissipation of $PM_{2.5}$ in the RP stage (with negative TFI) was mainly from north to south, with an average transport height of ~1 km above the surface. Our results quantified the multi-dimensional distribution and evolution of $PM_{2.5}$ concentration over the NCP, which may help policymakers develop efficient air pollution control strategies.

https://doi.org/10.5194/acp-2020-1273
Preprint. Discussion started: 8 January 2021

Atmospheric Chemistry and Physics Discussions

1 Introduction

Frequent heavy air pollution has exerted significant impacts on air visibility, climate, human health, and other environmental concerns (Gao et al., 2017a; Pokharel et al., 2019; Su et al., 2020). As a developing country with the largest population in the world, China's air quality has exhibited an obvious improvement trend in recent years (Cao et al., 2017; Zhang and Cao, 2015). Regional air pollution in China is still serious, however, especially the heavy aerosol pollution (HAP) caused by fine particulate matter ($PM_{2.5}$) in winter, which has attracted attention worldwide (Cheng et al., 2016; Li et al., 2017b; Zheng et al., 2015; Zheng et al., 2019). Therefore, providing a reliable distribution of the $PM_{2.5}$ concentration of HAP, especially at any time and at any height in a given region, is particularly important in the quest of the public to avoid health problems and to provide government policy makers with help in designing effective controls (Hu et al., 2015).

Compared with other air pollutants (e.g., ozone and nitrogen dioxide), $PM_{2.5}$ has a longer atmospheric lifetime (3–5 days), during which it can be transported vertically to great heights and horizontally hundreds of kilometers (Wang et al., 2017; Zhang et al., 2014), depending on the meteorological conditions (e.g., relative humidity and precipitation) and chemical composition (Yang et al., 2017). Previous study demonstrated that regional transport plays an important role for pollution formation in major cities of China, e.g., transport contributes over 50% of the $PM_{2.5}$ mass concentration in Beijing city, Shanghai city, Hangzhou city, Guangzhou city, Hong Kong and Chengdu city during the relatively polluted period (Sun et al., 2017). From 2005–2010, annually, about 35.5% (32.8 $\mu g \cdot m^{-3}$) of the $PM_{2.5}$ in Beijing was attributed to regional transport from the North China Plain (NCP), within which up to 60.4% (64.3 $\mu g \cdot m^{-3}$) from southerly and westerly air flows (Wang et al., 2015). Since the 2013 implementation of the most stringent clean air policy in China, the control of local pollution sources has led to the rapid reduction of total $PM_{2.5}$ concentration (Zhang et al., 2019c). It should be noted, however, that the local contributions, intra-regional transport, and inter-regional transport accounted for 47% (12.7 $\mu g \cdot m^{-3}$), 25% (6.6 $\mu g \cdot m^{-3}$), and 28% (7.6 $\mu g \cdot m^{-3}$), respectively, of the total $PM_{2.5}$ for the Beijing-Tianjin-Hebei (BTH) region from 2014–2017, with the 2017 contribution of regional transport to the BTH concentration rate ranging from 32.5–68.4% (Dong et al., 2020).

Previous studies have shown that it is difficult to use surface observations to characterize the impact of upper-level pollutants in the atmosphere (Huang et al., 2018b), which is affected by local emissions, regional transport, meteorological conditions, geographical factors etc.

https://doi.org/10.5194/acp-2020-1273
Preprint. Discussion started: 8 January 2021

(Tao et al., 2020). Therefore, understanding the key processes that drive the dynamic temporal and spatial evolutionary characteristics of pollutants on the NCP is essential for revealing the source and transport of aerosols, which has different radiative forcing at different heights (Kumar et al., 2017). Actually, stereo-monitoring devices and technologies, such as lidar (Chen et al., 2019b; Fan et al., 2019; Sheng et al., 2019), MAX-DOAS (Hong et al., 2018; Zhang et al., 2020), and satellite remote sensing (Pang et al., 2018; Schwartz et al., 2012; Zhang et al., 2019a), can reveal the vertical distribution of pollutants at different heights (Heese et al., 2017; Tian et al., 2017). Due to the limited spatial and temporal observations, however, it is impossible to provide physical and chemical properties in the atmosphere at any time period and on any path, which makes it difficult to directly reveal the formation and source of pollution.

On the other hand, although the distribution of pollutants can be simulated by air quality models (Huang et al., 2018a; Zhang et al., 2008), large uncertainties remain, mainly from the influence of emission inventory, meteorological fields, and some hypothetical conditions (Chen et al., 2017; Huang et al., 2016; Xu et al., 2016). Fortunately, the above observed data and the results of the model can be fused using data assimilation techniques, which can correct the model simulation results via the observed data (Ma et al., 2019; Wang et al., 2013). Research has shown that mainstream data assimilation (DA) technologies, including 3DVAR (Jiang et al., 2013; Ma et al., 2018), 4DVAR (Yumimoto et al., 2008), and EnKF (Chen et al., 2019a), can be used to assimilate observation data from the surface, remote sensing data (such as AOD) from satellites, and vertical profile data from lidar, all of which can be used to improve the performance of the model, including the simulation of $PM_{2.5}$ and PM_{10}.

In this study, we analyzed the observation data from a vertical observation network consisting of 13 lidars and surface observation stations during an extreme pollution event in eastern China, especially in the NCP. Next, all of the data were utilized by the Gridpoint Statistical Interpolation (GSI) three-dimensional (3-D) variational (3DVAR) data assimilation system to revise the $PM_{2.5}$ results from the WRF-Chem simulation (Pagowski et al., 2014). Finally, the multi-dimensional evolutionary characteristics of $PM_{2.5}$ at the surface and in the vertical layer, as well as the 3-D distribution, were analyzed in detail. Although data assimilation has been applied in China using surface observation network data (Gao et al., 2017b), AOD (Liu et al., 2011; Saide et al., 2013; Saide et al., 2014; Schwartz et al., 2012), and lidar data (Cheng et al., 2019), to our knowledge, this is the first attempt in China to apply lidar network data to assimilation technology, from which the high-precision 3-D distribution of pollutants can be provided, thus supplying effective data support for clarifying the formation mechanism of pollutants (Zheng et al., 2017).

https://doi.org/10.5194/acp-2020-1273
Preprint. Discussion started: 8 January 2021

Atmospheric Chemistry and Physics Discussions

2 Measurements and methods

2.1 Lidar observation network

The vertical aerosol observation network of the NCP was composed of 13 aerosol lidar monitoring stations (Fig. 1), covering four main transport channels of Beijing pollutants, including the southwestern transport path of Baoding City (BD), Shijiazhuang City (SJZ), Xingtai City (XT), Handan City (HD), Xinxiang City (XX), and Yangquan City (YQ); the southern transport path of Dezhou City (DZ) and Jining City (JN); the southeastern transport path of Langfang City (LF), Cangzhou City (CZ), and Zibo City (ZB); the eastern transport path of Tianjin City (TJ); and a lidar in the urban area of Beijing (BJ).

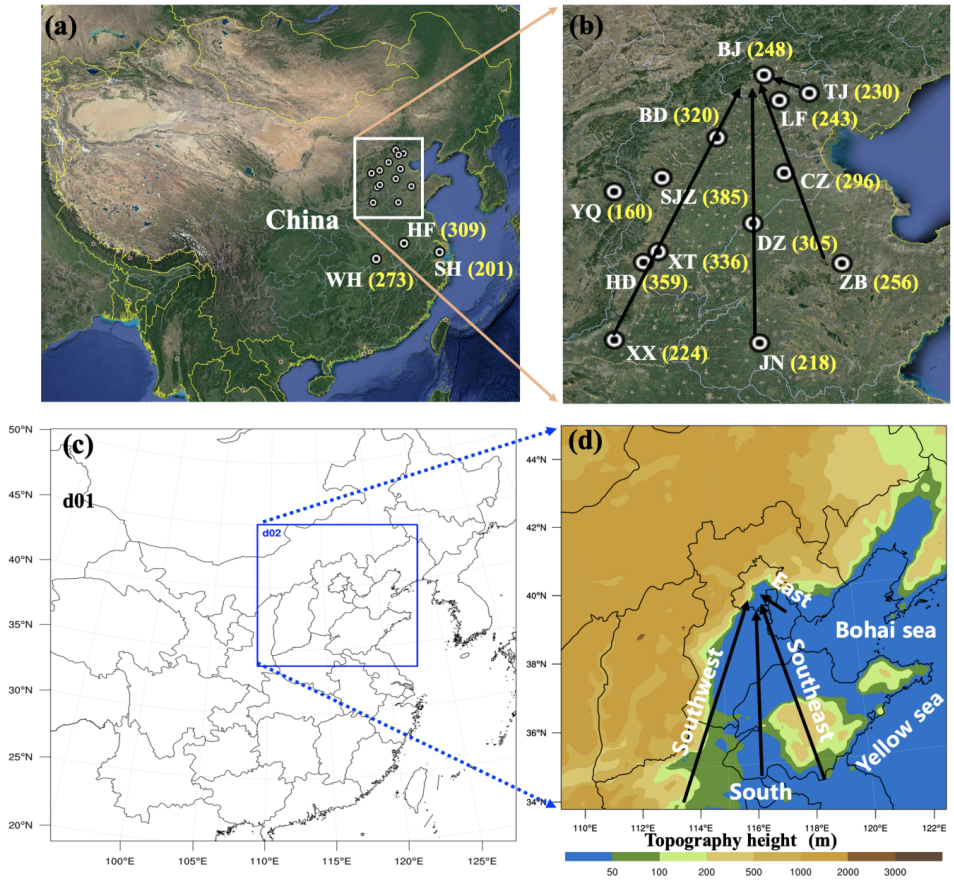

Figure 1. © Google maps of (a) China with the studied cities and (b) the North China Plain with all the lidar stations. The data in brackets are the maximum $PM_{2.5}$ concentrations ($\mu g \cdot m^{-3}$) at the surface during the observation period. (c) Two-nested WRF-Chem modeling domains and (d) topographic elevation data in d02. The black arrows in (b, d) from left to right show that the main pollution pathways of Beijing come from the four directions of southwest, south, southeast, and east.

https://doi.org/10.5194/acp-2020-1273
Preprint. Discussion started: 8 January 2021


Atmospheric Chemistry and Physics Discussions

The lidar system was developed by the Anhui Institute of Optics and Fine Mechanics (AIOFM), Chinese Academy of Sciences (CAS), and was used for the long-term continuous observation of aerosol vertical distribution. The lidar system adopted the Nd: YAG laser, which emits a 532-nm wavelength, with 30-mJ single-pulse energy and 10–30-Hz pulse repetition frequency. The vertical resolution is 7.5 m, with a time resolution of 3–10 min. The detection blind area is 0.1 km; more specific technical details can be found in other literature (Xiang et al., 2019). The vertical distribution of the aerosol extinction coefficient was retrieved using the Fernald method (Fernald, 1984), which is more suitable for vertical detection and more accurate than the Collis (Collis et al., 1964) and Klett (Klett, 1981) methods (Lu et al., 2015). Furthermore, combining the extinction coefficient with the $PM_{2.5}$ *in-situ* surface observations, the vertical distribution of the $PM_{2.5}$ mass concentration in the boundary layer was obtained using the empirical formula fitting method, which has proven to be reliable and highly accurate; the specific technical details can be found in other literature (Lv et al., 2017a; Lv et al., 2017b; Tao et al., 2016). In addition, an image recognition algorithm was used to evaluate the height of the atmospheric boundary layer (Barrera et al., 2019; Xiang et al., 2019).

2.2 WRF-Chem model configurations

The WRF-Chem chemical transport model was used to investigate the particulate concentrations and meteorological parameters in the study area and was configured with nested domains consisting of 100 × 100 (36 km) and 103 × 103 (12 km) grids (Figs. 1c and 1d). The domain had 41 vertical layers from the surface to 50 hPa. To better simulate the conditions within the boundary layer, the resolution of the boundary layer was increased, and 20 layers were set in the range of 0–2 km. The initial and boundary meteorological conditions were derived from the 6-h National Centers for Environmental Prediction Final Analysis data with 1° × 1° spatial resolution. The inventory of anthropogenic emissions for 2016 was obtained from the Multi-resolution Emission Inventory for China (MEIC) data with 0.25° × 0.25° resolution (Zhou et al., 2017). Terrestrial biogenic emissions were estimated using the Model of Emissions of Gases and Aerosols from Nature (MEGAN) model (Chatani et al., 2011). The gas-phase chemistry module CBM-Z and the Model for Simulating Aerosol Interactions and Chemistry (MOSAIC) aerosol module were used in this simulation. Detailed information concerning the model configuration is provided in Table S1. The model runs from November 20, 2017–December 9, 2017, and the results from November 25–December 9, 2017 were used for the analysis in Section 3.

2.3 GSI 3DVAR DA system

https://doi.org/10.5194/acp-2020-1273
Preprint. Discussion started: 8 January 2021

Atmospheric Chemistry and Physics Discussions

The GSI DA (Gridpoint Statistical Interpolation Data Assimilation) system provides 3DVAR analysis by minimizing the cost function as shown below (Gao et al., 2017b):

$$J(x) = (x - x_b)^T B^{-1}(x - x_b) + \left(y - H(x)\right)^T R^{-1}\left(y - H(x)\right) \quad (1)$$

In this equation, x is the analysis vector, x_b denotes the background vector, y is an observation vector, B represents the background error covariance matrix, R represents the observation error covariance matrix, and H is the observation operator used to transform model grid point values to observed variables, which was performed via interpolation in our research. The background error covariance matrix was calculated using the National Meteorological Center (NMC) method (Parrish and Derber, 1992; Saide et al., 2013), which simulated the difference of results at the same time (November 25, 2017) with two different starting times (November 20, 2017 and November 21, 2017, respectively). The 1-hour assimilated window data included 13 groups (see Fig. 1 for site distribution) of $PM_{2.5}$ vertical profiles retrieved from lidar, and the surface $PM_{2.5}$ data from hundreds of surface monitoring stations (see Fig. 5 for site distribution) from the China Environmental Monitoring Center. The observation errors of $PM_{2.5}$ ground and its vertical distribution (through the ground $PM_{2.5}$ fitting method in Section 2.1) originated from measurement errors and representative errors. The measurement error was computed using $\varepsilon_0 = 1.5 + 0.0075 * obs$ (Pagowski et al., 2014), where *obs* indicates observed values. The representative error was computed using $\varepsilon_r = \gamma\varepsilon_0\sqrt{\Delta x/L}$ (Elbern et al., 2007), where γ is the adjustable scale factor (we used the value of 0.5 recommended by the GSI system), Δx is the model grid resolution (we selected 12 km of domain 2), and L is the influencing radius (we used 60 km).

3 Results and discussion

3.1 Evaluation of assimilation performance using vertical $PM_{2.5}$ data

In order to evaluate the improvement of model simulation performance from data assimilation using lidar vertical profile data and surface station data, considering the sharp decline of $PM_{2.5}$ value at 1km height (Fig. 6), only the non-assimilation and assimilation results at the surface, 0.2 km, 0.5 km, and 1 km were compared, as shown in Fig. 2. These data were selected from five of the most polluted stations, including the cities of TJ, LF, BD, SJZ, and XT. It should be noted that these observation data were not assimilated, which means that the following comparisons are independent (Bocquet et al., 2015). Obviously, the data assimilation used can greatly improve the simulation accuracy. Compared with the observation data at different heights, the simulation results of $PM_{2.5}$ levels under the condition of non-assimilation were higher (Figs. 2 a–d), the root-mean-square error (RMSE) was 52.14 ± 20.27 $\mu g \cdot m^{-3}$, and

https://doi.org/10.5194/acp-2020-1273
Preprint. Discussion started: 8 January 2021

Atmospheric Chemistry and Physics Discussions

the correlation coefficient was only 0.56 ± 0.15. Correspondingly, the results of $PM_{2.5}$ simulated with assimilation were closer to the observed values (Figs. 2 e–h), the RMSE was 33.07 ± 14.69 $\mu g \cdot m^{-3}$, which represents a reduction of about 40% in simulation error after assimilation. The correlation coefficient was 0.81 ± 0.10, demonstrating that the simulation accuracy was improved by about 50% after assimilation.

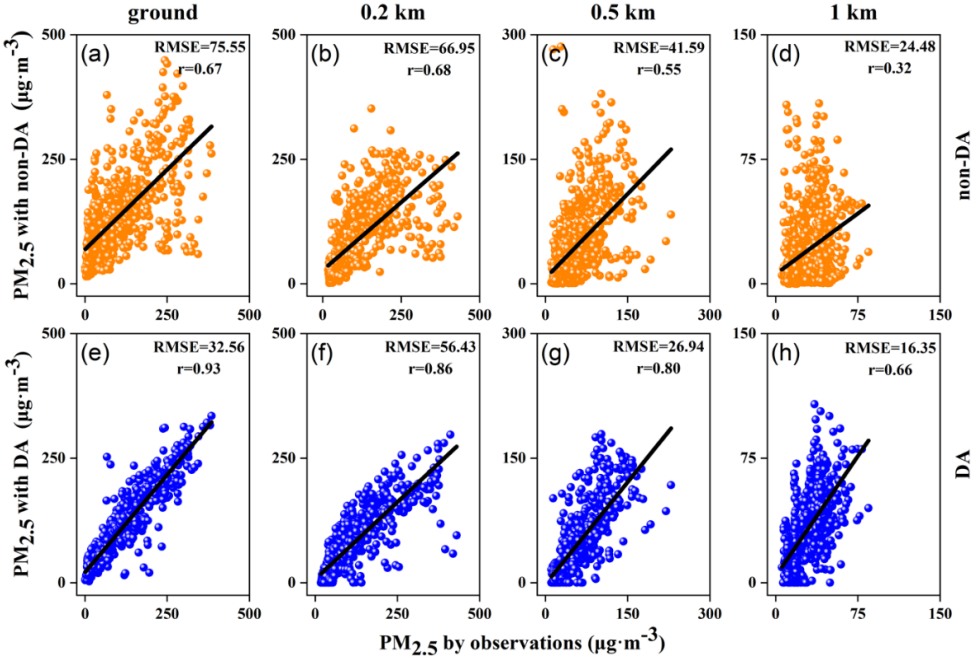

Figure 2. $PM_{2.5}$ mass concentration comparison results from lidar at different heights (b–d, f–h) and surface observations (a, e) with non-assimilation simulations (a–d) and assimilation simulations (e–h).

In addition, compared with the simulation with assimilation (Fig. 5 in Section 3.3), the results without assimilation were significantly higher than the observed values (Fig. S1), especially during the pollution period (Figs. S1d, S1e), which may be due to the simulation error caused by the model (Zhang et al., 2016). Meanwhile, the comparison of the three-dimensional results (Fig. 7 in Section 3.5 and Fig S2) further reveals that the simulation results of upper air $PM_{2.5}$ may also overestimate the actual values, which demonstrates the importance of data assimilation in capturing the three-dimensional structure of pollution.

3.2 The four phases from aerosol pollution development to dissipation

Joint observations and analyses have been widely performed in an effort to reveal the heavy aerosol pollution (HAP) in the NCP region (Li et al., 2016; Zhang et al., 2018). The key processes of a HAP event, from aerosol pollution development to dissipation, usually include

https://doi.org/10.5194/acp-2020-1273
Preprint. Discussion started: 8 January 2021

Atmospheric Chemistry and Physics Discussions

an early phase (EP), a transport phase (TP), an accumulation phase (AP), and a removal phase (RP) (Yuan et al., 2019; Zhong et al., 2017), classifications that are based on the increase and decrease of $PM_{2.5}$ mass concentration in Beijing (BJ) caused by changes in meteorological conditions. Here, the curves in Fig. 3 shows the temporal evolution of $PM_{2.5}$ mass concentration monitored at the surface in different cities on the NCP from November 25–December 9, 2017, while the superimposed colors represent the time-varying profiles of the simulated wind fields in BJ, Baoding (BD), Dezhou (DZ), and Langfang (LF), respectively. Overall, $PM_{2.5}$ with high concentrations was usually associated with pronounced southerly winds (S in Fig. 3) or southwesterly winds (SW in Fig. 3), while the $PM_{2.5}$ concentrations decreased significantly under the prevailing northerly winds (including the wind directions of N, NW, and NE in Fig. 3).

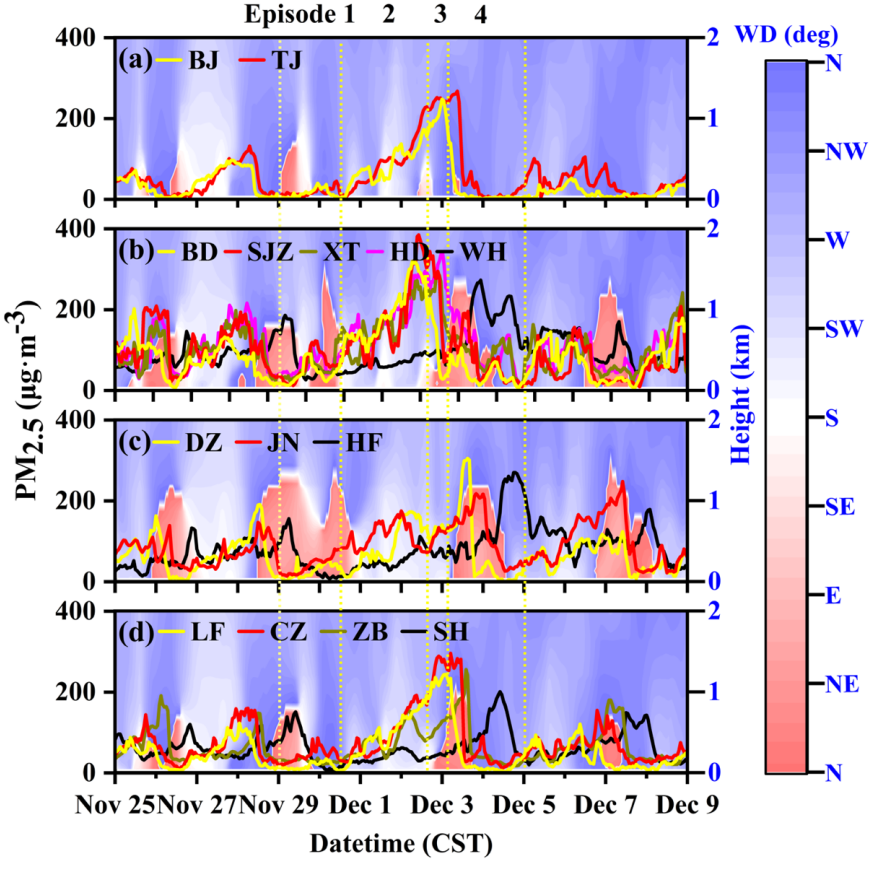

Figure 3. Surface $PM_{2.5}$ observations from different cities: (a) Beijing (including Tianjin) and its (b) southwest cities, (c) southeast cities, and (d) east cities for the period November 25–December 9, 2017. Superimposed colors represent the time-varying profiles of the simulated wind fields in Beijing, Baoding, Dezhou, and Langfang, respectively.

https://doi.org/10.5194/acp-2020-1273
Preprint. Discussion started: 8 January 2021

Atmospheric Chemistry and Physics Discussions

Furthermore, in order to characterize the evolution of $PM_{2.5}$ during different pollution phases, the period from November 29–December 5 was selected as a typical extreme HAP event covering the four pollution phases. This extreme pollution event lasted more than 4 days and featured a regional transport process. During the EP (November 29–noon November 30; episode 1 in Fig. 3), the air quality in BJ and its surrounding areas such as Tianjin (TJ) was relatively good, with an average $PM_{2.5}$ value of ~15 $\mu g \cdot m^{-3}$, while slight pollution occurred to the southwest of BJ, including BD, Shijiazhuang (SJZ), Xintai (XT), and Handan (HD), with an average value of ~50 $\mu g \cdot m^{-3}$.

During the TP (approximately the morning of December 2; episode 2 in Fig. 3), the variation of $PM_{2.5}$ concentration was more sensitive and responded rapidly to the wind shift from northerly to southerly, causing the $PM_{2.5}$ concentration in Beijing to increase quickly from ~30 $\mu g \cdot m^{-3}$ to ~150 $\mu g \cdot m^{-3}$, while southwest of Beijing (e.g., BD, SJZ, XT, and HD) the $PM_{2.5}$ concentration increased rapidly to ~200 $\mu g \cdot m^{-3}$. Research has revealed that the pollutant transport south of Beijing, especially in the southwest areas (the Taihang Mountains), is the most important contribution source of Beijing pollutants (Zhao et al., 2020). During the AP (approximately December 3; episode 3 in Fig. 3), diffusion of the pollutants was difficult due to the occurrence of a surface temperature inversion in Beijing (Fig. 4) (Wang et al., 2019), which caused the maximum concentration of $PM_{2.5}$ in Beijing to reach ~250 $\mu g \cdot m^{-3}$. Meanwhile, the $PM_{2.5}$ concentrations in TJ, LF, BD, and SJZ reached maximum values of ~270, 250, 320, and 390 $\mu g \cdot m^{-3}$, respectively. Conversely, the pollution levels in Shanghai (SH), Hefei (HF), and Wuhan (WH) in the southernmost section of the NCP were relatively low, with average values < ~60 $\mu g \cdot m^{-3}$.

During the RP (approximately December 5; episode 4 in Fig. 3), the wind direction shifted from southwest to north, transporting the relatively clean air in the north to the south, and thereby causing the pollutant concentrations in Beijing to decrease rapidly. In just 9 hours, the air quality improved from heavy pollution to excellent, and the $PM_{2.5}$ concentrations in the NCP also decreased significantly. Finally, by noon on December 4, the pollutant concentrations in the NCP had reached a low level, with an average value of ~40 $\mu g \cdot m^{-3}$. In contrast, due to the continuous southward advection of pollutants, serious pollution occurred in SH, HF, and WH, where the $PM_{2.5}$ concentrations reached maximum values of ~210, 310, and 280 $\mu g \cdot m^{-3}$, respectively. These findings are also consistent with the results of previous studies on the regional transport of regional pollutants to the Yangtze River Delta (Hua et al., 2015), which showed them to be due to the continuous southward flow of northwest and northeast winds.

https://doi.org/10.5194/acp-2020-1273
Preprint. Discussion started: 8 January 2021

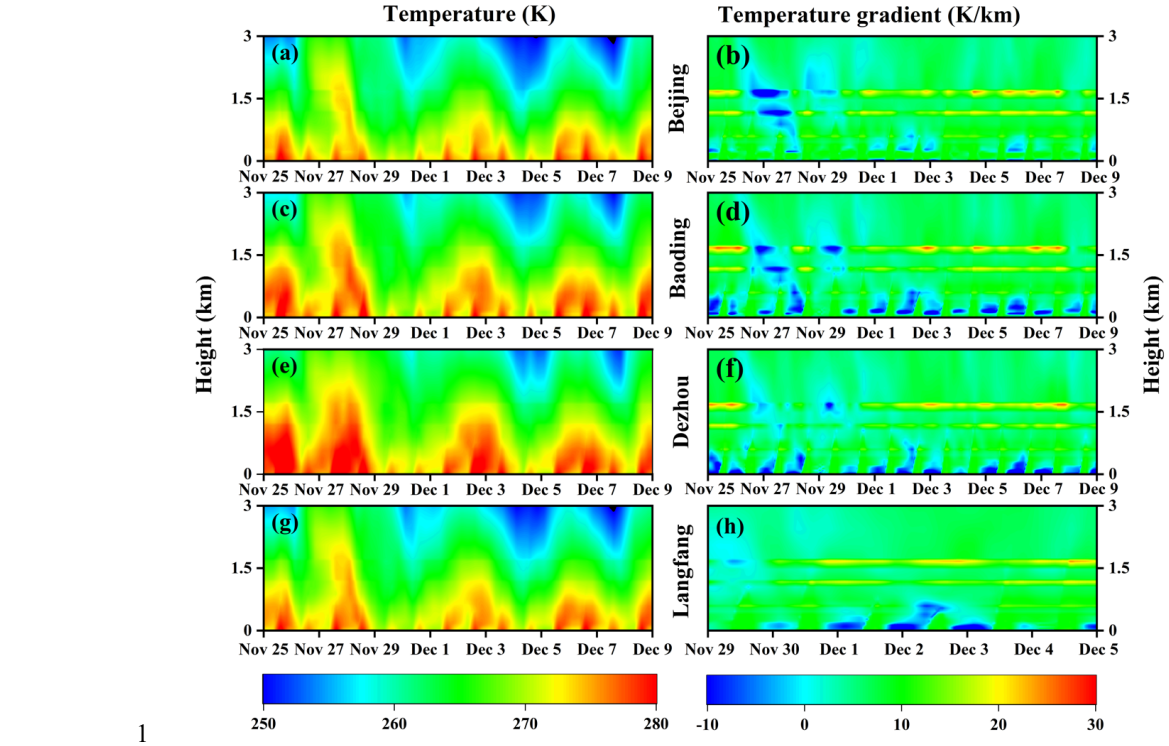

Figure 4. Time series of vertical temperatures (a, c, e, g) and temperature gradients (b, d, f, h) from Beijing (a, b), Baoding (c, d), Dezhou (e, f), and Langfang (g, h) simulated by the WRF-Chem model.

3.3 Spatial distribution of $PM_{2.5}$ concentration in the surface layer

Additionally, in order to analyze the pollution characteristics of the NCP, the spatial distribution results of $PM_{2.5}$ after data assimilation were plotted in Fig. 5 for all phases. The high concentrations of $PM_{2.5}$ in BJ were recorded during the TP, AP, and beginning of the RP, while the $PM_{2.5}$ concentrations at other times were lower. Moreover, during the EP, only the eastern cities of Shanxi (SX) Province experienced moderate pollution levels (Fig. 5a). During the TP, the pollutants in the south-central NCP were transported to the north of the NCP (Figs. 5b and c) as a result of the southwesterly wind field, and under the superposition of the local pollutant emissions from each city (Li et al., 2017a), the cities on the windward side of the Taihang Mountains (e.g., HD, SJZ, and BD) quickly developed varying levels of heavy pollution. In addition, during the AP, due to the large-scale inversion (Figs. 4b, d, f, h) caused by the rapid temperature rise (Figs. 4a, c, e, g) of the NCP region at upper levels, the atmospheric stratification was stable, causing the pollutant loading on the NCP (including BJ, BD, SJZ, HD, LF, CZ, and elsewhere) to increase (Fig. 5d), nearly reaching their pollution maxima (Fig. 3). Meanwhile, during the RP, affected by the cold air at upper levels (Figs. 4a,

https://doi.org/10.5194/acp-2020-1273
Preprint. Discussion started: 8 January 2021

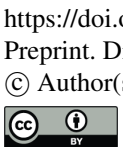

Atmospheric Chemistry and Physics Discussions

c, e, g) from the northwest and the shift in wind direction over the NCP from southwest to north, the pollution severity gradually eased from north to south (Fig. 5e), with the air quality in the northern part of the region improving significantly (Fig. 5f).

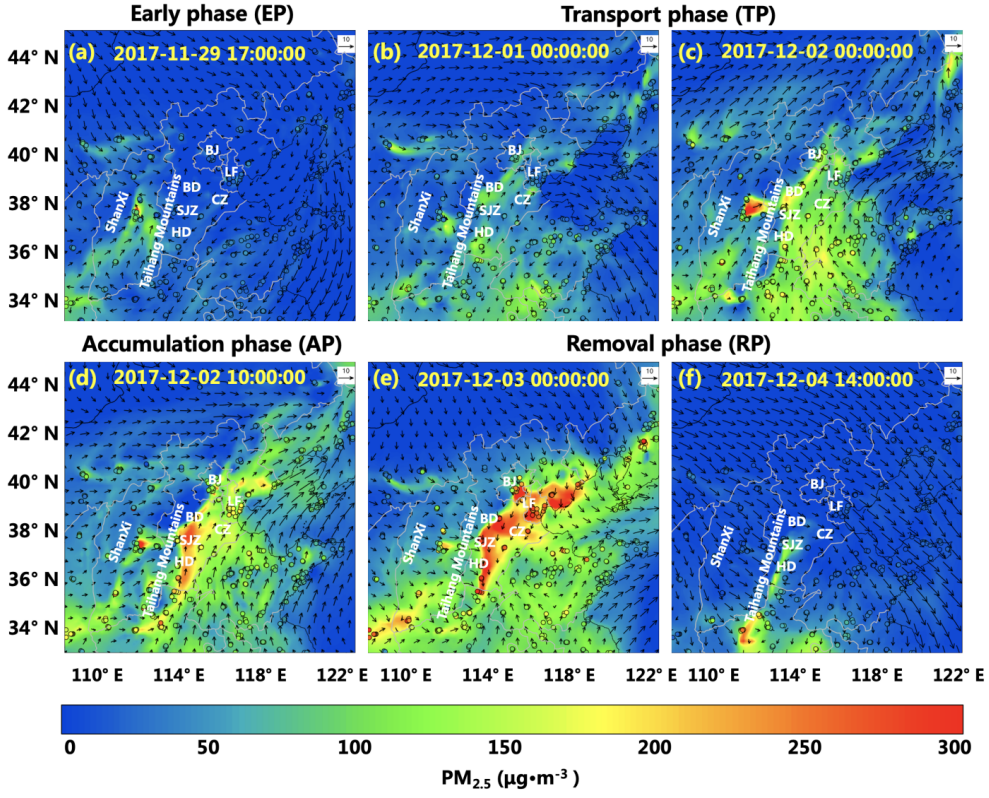

Figure 5. Spatial distribution of $PM_{2.5}$ in the surface layer during different phases after assimilation. The black arrows indicate the wind direction. The circles represent the *in-situ* surface observations.

3.4 Vertical distribution of aerosols observed by the lidar network

In order to quantify the characteristic vertical distribution of aerosols, the observed aerosol extinction coefficients from the 13 lidar stations in the NCP were plotted, as shown in Fig. 6. These results revealed that on November 29, the aerosol concentration at the surface was relatively low, although pollutant transport at heights of 1–2 km (see Figs. 8a, e) occurred at six stations (BD, SJZ, YQ, XT, HD, and XX) on the windward side of the Taihang Mountains. The upper air transport of pollutants continued until December 1, at which it merged with the surface flow. Contrary to this, the pollutant transport from north to south occurred at a height of 1 km during the RP (e.g., Figs. 6b, d–g). In addition, the atmospheric boundary layer height (ABLH) reached its highest value of the observation period from November 29 to 30, averaging more than 1.5 km. The ABLH began to decrease on December 1, averaging approximately 1

https://doi.org/10.5194/acp-2020-1273
Preprint. Discussion started: 8 January 2021

Atmospheric Chemistry and Physics Discussions

km on that day. The lowest value of the ABLH occurred on December 2–3, when its average dropped to less than 0.5 km, making it difficult for pollutants to diffuse and causing heavy pollution in the NCP (Li et al., 2017c). Fortunately, on December 4, the atmospheric boundary layer gradually lifted, which was conducive to the diffusion of pollutants.

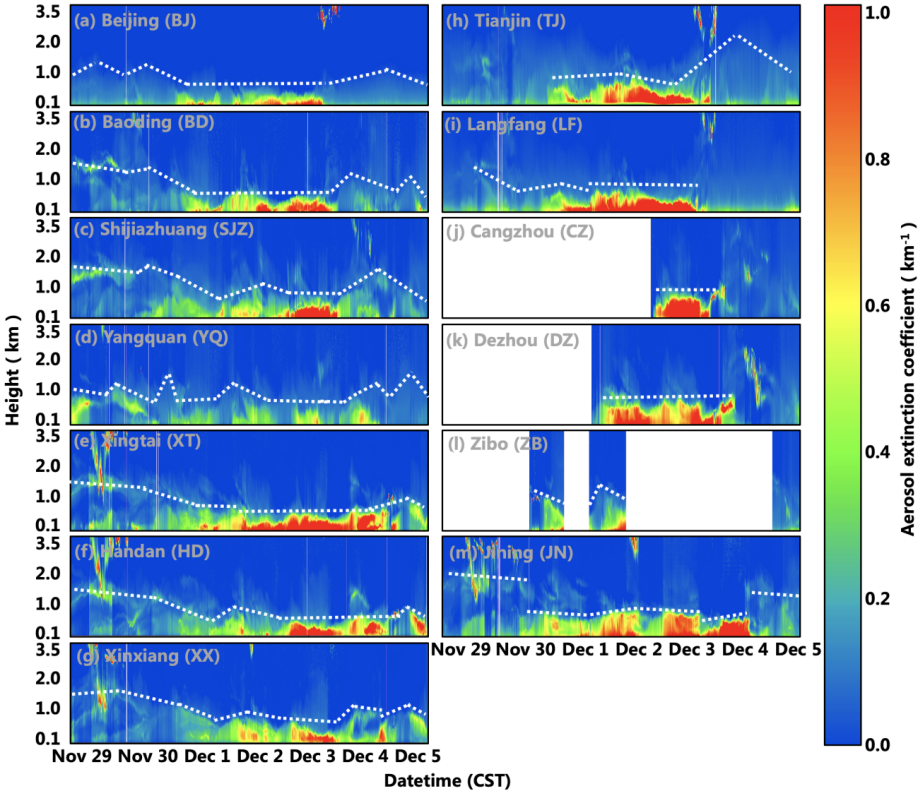

Figure 6. Time series of vertical distributions of the aerosol extinction coefficient observed on the North China Plain from November 29–December 5, 2017. The white dashed lines represent the approximate atmospheric boundary layer height.

3.5 Dynamic 3-D evolution of the $PM_{2.5}$ concentrations

Figure 7 presents the 3-D distribution of $PM_{2.5}$ after assimilation, which clearly shows the generation, dissipation, transport, and diffusion characteristics of pollutants in the atmosphere. The tops of the boxes in the figure depict the wind speeds 10 m above the surface. During the EP, the high-concentration pollutants only occurred in the upper air within ~1 km of the surface in SX Province (e.g., YQ). During the TP, the high-concentration pollutants were mainly found on the windward side of the Taihang Mountains (southwest pathway), and the loading height of $PM_{2.5}$ was < 1 km, which is illustrated in Fig. 8. During the AP, the average concentration of pollutants > 200 $\mu g \cdot m^{-3}$ mainly occurred near the surface. Meanwhile, the

https://doi.org/10.5194/acp-2020-1273
Preprint. Discussion started: 8 January 2021

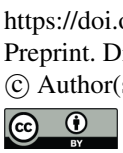

Atmospheric Chemistry and Physics Discussions

pollutants with low concentrations at upper levels could be transported to the Bohai Sea. During the RP, high-concentration pollutants > 100 μg·m^{-3} simultaneously occurred over the Bohai Sea and the Yellow Sea.

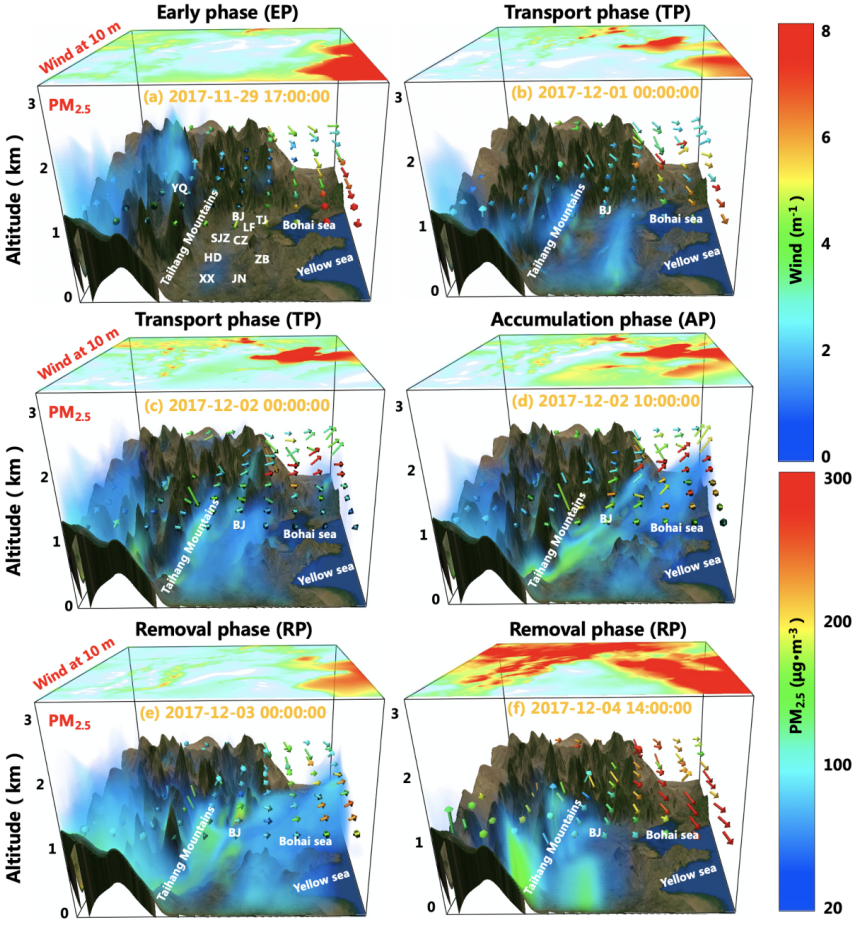

Figure 7. Three-dimensional distribution of $PM_{2.5}$ during different phases after assimilation. Colors within the boxes depict the $PM_{2.5}$ concentrations. The color-coded arrows represent the wind direction and speed at 1 km. On the tops of the boxes, the spatial distributions of wind speed at 10 m are plotted.

3.6 Quantification of regional transport of $PM_{2.5}$

To evaluate the variation of pollutants along different transport pathways at different stages, we plotted the vertical profile of the $PM_{2.5}$ cross-section along the main pollution pathways of Beijing come from the four directions of southwest, south, southeast, and east (see Figs. 1b, d). As shown in Fig.8, at XX and XT (located at the start of the southwest transport pathway, Fig. 8a), the $PM_{2.5}$ concentration is more than 200 μg·m^{-3} at a height of 1 km (Fig. 8a), and the surface $PM_{2.5}$ concentraiton at JN (located in the south pathway) also exceeds 200

https://doi.org/10.5194/acp-2020-1273
Preprint. Discussion started: 8 January 2021

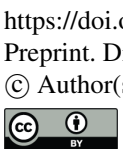

Atmospheric Chemistry and Physics Discussions

μg·m^{-3} (Fig. 8b). These high concentrations of pollutants were transported to SJZ, BD, LF, BJ, and other cities via southwest winds (Figs. 8e, f, g). At the same time, vertical downdrafts reduced the height of loading of aersol layer to ~0.6 km (Fig. 8e). Different from the southern (including southwest, south, and southeast) transport pathways, the pollutants in TJ were mainly from BJ outflow in all stages of the eastern transport pathways (Figs. 8d, h, l, p). In addition, wind direction inconsistencies at the origin (XX, JN, and ZB) and target location (Beijing) of the transport pathways occurred at the beginning of the removal phase (Figs. 8i–k), which may have been due to the southward delay of the northerly air flow.

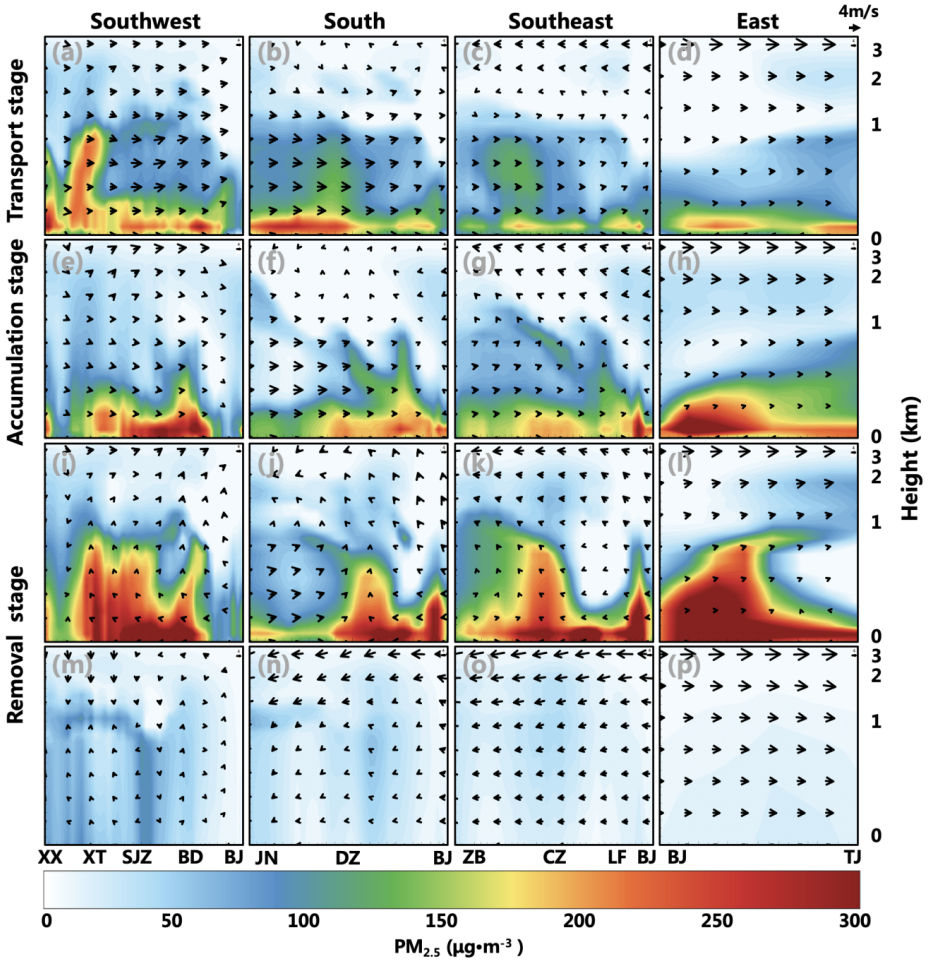

Figure 8. Vertical profiles of $PM_{2.5}$ cross-sections with wind vectors along the transport pathways, including southwest (first column), south (second column), southeast (third column), and east (fourth column). The first row (00:00 December 2, 2017) represents the transport stage, the second row (10:00 December 2, 2017) represents the accumulation stage, the third row (00:00, December 3, 2017) and the fourth row (14:00, December 4, 2017) represent the removal stage.

https://doi.org/10.5194/acp-2020-1273
Preprint. Discussion started: 8 January 2021

Atmospheric Chemistry and Physics Discussions

To investigate the vertical variation of $PM_{2.5}$ inflow or outflow at different heights and determine the height at which the main transport occurred (Zhang et al., 2019b), we plotted the vertical distribution of $PM_{2.5}$ transport flux in different directions (Fig. 9). Here the $PM_{2.5}$ transport flux is defined as the product of $PM_{2.5}$ mass concentration (μg m^{-3}), wind speed (m s^{-1}), and wind direction projection in the current pathway (Xiang et al., 2020). The southwest, southeast, and east pathways in Fig. 9 were represented by BD, LF, and TJ, respectively, which are the three lidar stations closest to BJ (Fig. 1). TF > 0 indicates that the pollutants were imported to Beijing, while TF < 0 indicates that the pollutants were exported from Beijing. The results revealed that below the height of 1.5 km, the order of the maximum values of imported pollutants to Beijing direction was southwest pathway (1122.8 μg m^{-2} s^{-1}) > southeast pathway (423.6 μg m^{-2} s^{-1}) > east pathway (278.3 μg m^{-2} s^{-1}), while the exported pollutants from Beijing direction was southwest pathway (-1571.4 μg m^{-2} s^{-1}) > east pathway (-877.7 μg m^{-2} s^{-1})> southeast pathway (-772.4 μg m^{-2} s^{-1}). Compared with the $PM_{2.5}$ transport flux on the ground surface, the relatively high value (~ 200 μg m^{-2} s^{-1}) in the southwest pathway (Fig. 9a) occurred on November 29 and early morning on December 4, while the relatively extreme value (~ -400 μg m^{-2} s^{-1}) on the east pathway (Fig. 9c) was recorded at the night of December 2.

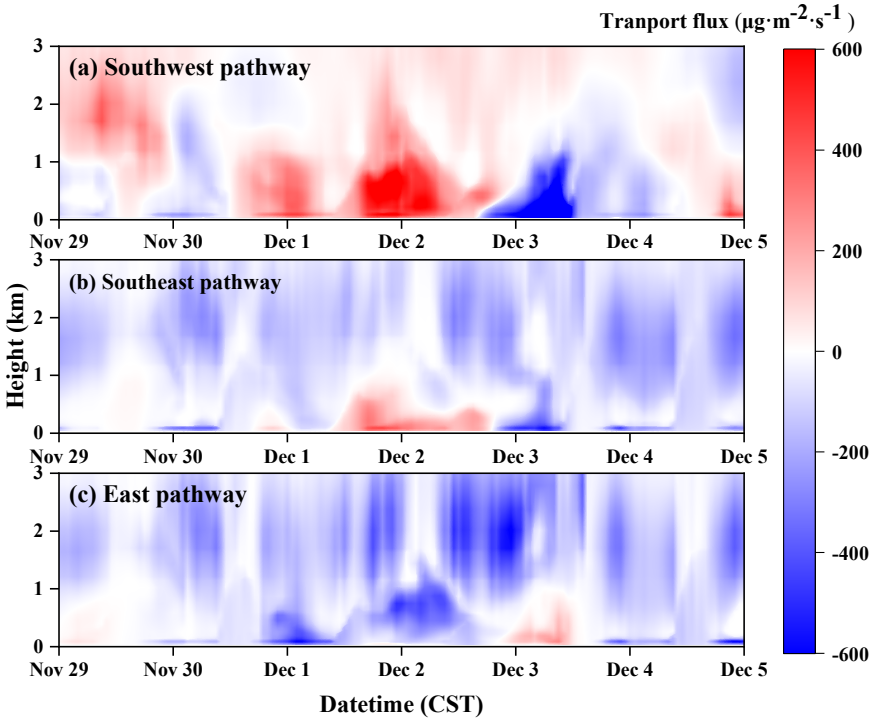

Figure 9. Time series of $PM_{2.5}$ transport flux from different transport pathways. The corresponding directions of the southwest, southeast, and east pathways are shown in Fig. 1.

https://doi.org/10.5194/acp-2020-1273
Preprint. Discussion started: 8 January 2021

Atmospheric Chemistry and Physics Discussions

To further obtain insights into the total transport characteristics in the target area (BJ) and its surrounding area (BD, LF, and TJ) during different evolutionary stages, the time series of the $PM_{2.5}$ transport flux intensity (TFI) was shown in Fig. 10, which was calculated by integrating the $PM_{2.5}$ transport flux within the height range of 1.5 km. The TFI of $PM_{2.5}$ further reveals that pollutants imported into the Beijing area with a maximum $PM_{2.5}$ TFI of ~4.6×10^5 $\mu g \cdot m^{-1} \cdot s^{-1}$ were transported mainly via the southwest pathway during the TP, while the extreme TFI of pollutants exported from Beijing via the east pathway was approximately -1.4×10^5 $\mu g \cdot m^{-1} \cdot s^{-1}$. In addition, during the RP, the pollutants from Beijing were exported to the southwest and southeast, with extreme values of approximately -1.03×10^6 and -4.3×10^5 $\mu g \cdot m^{-1} \cdot s^{-1}$, respectively. On the contrary, the absolute value of TFI on the southwest pathway was < ~1.0×10^4 $\mu g \cdot m^{-1} \cdot s^{-1}$ during the EP (Fig. 10), which indicates that there was no significant inflow or outflow of pollutants. However, this reason was mainly due to the offsetting of the inflow of pollutants in the upper-air and the outflow of pollutants near the ground (Fig. 9a). This special phenomenon also demonstrates that the study of vertical distribution of pollutants has great significance, which can better explain the transport characteristics (Zhang et al., 2019b).

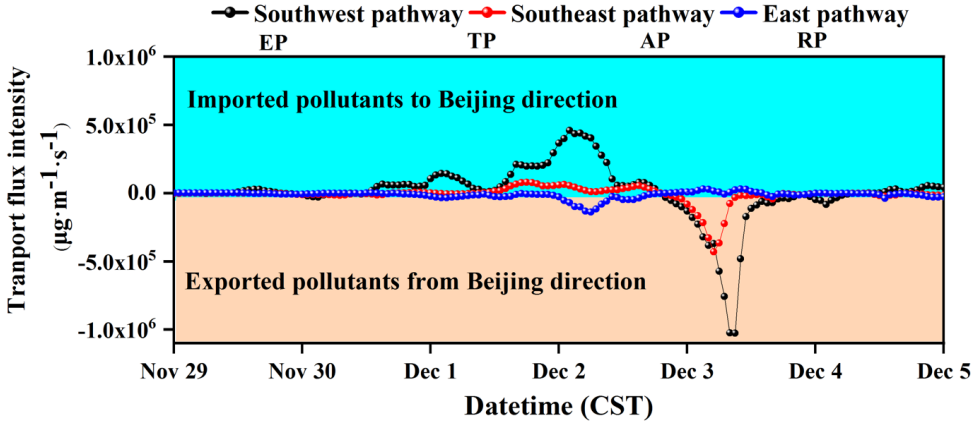

Figure 10. Time series of $PM_{2.5}$ transport flux intensity from different transport pathways. The corresponding directions of the southwest, southeast, and east pathways are shown in Fig. 1.

4 Conclusions

Accurate quantification of the distribution of particulate matter in the atmosphere is a key requirement for predicting air quality and estimating atmospheric environmental capacity from atmospheric observations. We utilized a vertical observation network composed of 13 aerosol lidars, combined with data assimilation technology, to improve the simulation accuracy

https://doi.org/10.5194/acp-2020-1273
Preprint. Discussion started: 8 January 2021

Atmospheric Chemistry and Physics Discussions

of $PM_{2.5}$, and further analyzed the multi-dimensional evolutionary characteristics of pollutants in the surface layer, vertical layer, and 3-D space, thereby providing effective data support for clarifying the spatial transport characteristics of heavy pollution.

We found that the average height of the atmospheric boundary layer was < 0.5 km during the HAP period. We further demonstrated that the transport of pollutants in the NCP region was mainly via three pathways: southwest, southeast, and east. During the TP, the $PM_{2.5}$ advected into Beijing with a maximum transport flux intensity (TFI) of ~4.6×10^5 $\mu g \cdot m^{-1} \cdot s^{-1}$ was mainly via the southwest pathway, while the polluted air mass in the RP dissipated from Beijing via the southwest and southeast pathways, with extreme $PM_{2.5}$ TFI values of approximately -1.03×10^6 and -4.3×10^5 $\mu g \cdot m^{-1} \cdot s^{-1}$, respectively. In addition, the transport of regional pollutants to the Yangtze River Delta was due to the continuous southward flow of northwest and northeast winds. Our results directly revealed that pollutants in the North China Plain can be transported to the Yellow Sea and the Bohai Sea, providing a dataset for a further in-depth study of the mechanism of air pollution in the coastal areas of eastern China. This study also captured the regional transport of air pollutants stretching over 1000 km, proving the necessity and importance of the joint prevention and control of regional air pollution.

Data availability

The FNL data are available from the following website (https://rda.ucar.edu/datasets/ds083.2/). The data in this study are analyzed using the NCAR Command Language (http://www.ncl.ucar.edu/). The authors are gratefully acknowledging the China National Environmental Monitoring Center for providing monitoring data for the $PM_{2.5}$ (http://106.37.208.233:20035). The lidar data in this study are available upon request from the corresponding author (yxiang@ahu.edu.cn).

Author contributions

YX and TZ designed this study. YX wrote the manuscript; YC and CM edited it. LL and TZ helped to analyze the data. YC, CM, WL, and JL provided constructive comments on this study. All authors contributed to the discussion and final version of the manuscript.

Competing interests

The authors declare that they have no conflict of interest.

Acknowledgements

This work was supported by the National Natural Science Foundation of China (42005106, 41941011), and the National Key Project of MOST (2017YFC0213002,

https://doi.org/10.5194/acp-2020-1273
Preprint. Discussion started: 8 January 2021

2018YFC0213101, 2018YFC0213106, 2018YFC0213201), and the Major science and technology projects of Anhui Province (No.18030801111), and the Natural Science Foundation of Anhui Province, China (1908085QD160, 1908085QD170), and the Doctoral Scientific Research Foundation of Anhui University (Y040418190). The authors are grateful to the China National Environmental Monitoring Center for providing the $PM_{2.5}$ monitoring data. The authors also gratefully acknowledge © Google Earth for providing the map used in this research. Yafang Cheng and Chaoqun Ma thank the Minerva program of Max Planck Society.

References

Barrera YD, Nehrkorn T, Hegarty J, Sargent M, Benmergui J, Gottlieb E, et al. Using Lidar Technology To Assess Urban Air Pollution and Improve Estimates of Greenhouse Gas Emissions in Boston. Environ Sci Technol 2019; 53: 8957-8966. https://doi.org/10.1021/acs.est.9b00650

Bocquet M, Elbern H, Eskes H, Hirtl M, Zabkar R, Carmichael GR, et al. Data assimilation in atmospheric chemistry models: current status and future prospects for coupled chemistry meteorology models. Atmospheric Chemistry and Physics 2015; 15: 5325-5358. https://doi.org/10.5194/acp-15-5325-2015

Cao F, Zhang YL, Ren LJ, Liu JW, Li J, Zhang G, et al. New insights into the sources and formation of carbonaceous aerosols in China: potential applications of dual-carbon isotopes. National Science Review 2017; 4: 804-+. https://doi.org/10.1093/nsr/nwx097

Chatani S, Morikawa T, Nakatsuka S, Matsunaga S, Minoura H. Development of a framework for a high-resolution, three-dimensional regional air quality simulation and its application to predicting future air quality over Japan. Atmospheric Environment 2011; 45: 1383-1393. https://doi.org/10.1016/j.atmosenv.2010.12.036

Chen D, Liu ZQ, Ban JM, Chen M. The 2015 and 2016 wintertime air pollution in China: SO2 emission changes derived from a WRF-Chem/EnKF coupled data assimilation system. Atmospheric Chemistry and Physics 2019a; 19: 8619-8650. https://doi.org/10.5194/acp-19-8619-2019

Chen DS, Liu XX, Lang JL, Zhou Y, Wei L, Wang XT, et al. Estimating the contribution of regional transport to PM2.5 air pollution in a rural area on the North China Plain. Science of the Total Environment 2017; 583: 280-291. https://doi.org/10.1016/j.scitotenv.2017.01.066

Chen Z, Schofield R, Rayner P, Zhang T, Liu C, Vincent C, et al. Characterization of aerosols over the Great Barrier Reef: The influence of transported continental sources. Sci Total Environ 2019b; 690: 426-437. https://doi.org/10.1016/j.scitotenv.2019.07.007

Cheng X, Liu Y, Xu X, You W, Zang Z, Gao L, et al. Lidar data assimilation method based on CRTM and WRF-Chem models and its application in PM2.5 forecasts in Beijing. Sci Total Environ 2019; 682: 541-552. https://doi.org/10.1016/j.scitotenv.2019.05.186

Cheng YF, Zheng GJ, Wei C, Mu Q, Zheng B, Wang ZB, et al. Reactive nitrogen chemistry in aerosol water as a source of sulfate during haze events in China. Science Advances 2016; 2,e1601530. https://doi.org/10.1126/sciadv.1601530

Collis RTH, Fernald FG, Ligda MGH. Laser Radar Echoes from a Stratified Clear Atmosphere. Nature 1964. https://doi.org/10.1038/2031274a0

Dong Z, Wang S, Xing J, Chang X, Ding D, Zheng H. Regional transport in Beijing-Tianjin-Hebei region and its changes during 2014-2017: The impacts of meteorology and

https://doi.org/10.5194/acp-2020-1273
Preprint. Discussion started: 8 January 2021

emission reduction. Sci Total Environ 2020; 737: 139792. https://doi.org/10.1016/j.scitotenv.2020.139792

Elbern H, Strunk A, Schmidt H, Talagrand O. Emission rate and chemical state estimation by 4-dimensional variational inversion. Atmospheric Chemistry and Physics 2007; 7: 3749-3769. https://doi.org/DOI 10.5194/acp-7-3749-2007

Fan WZ, Qin K, Xu J, Yuan LM, Li D, Jin Z, et al. Aerosol vertical distribution and sources estimation at a site of the Yangtze River Delta region of China. Atmospheric Research 2019; 217: 128-136. https://doi.org/10.1016/j.atmosres.2018.11.002

Fernald FG. Analysis of Atmospheric Lidar Observations - Some Comments. Applied Optics 1984; 23: 652-653. https://doi.org/10.1364/Ao.23.000652

Gao JH, Woodward A, Vardoulakis S, Kovats S, Wilkinson P, Li LP, et al. Haze, public health and mitigation measures in China: A review of the current evidence for further policy response. Science of the Total Environment 2017a; 578: 148-157. https://doi.org/10.1016/j.scitotenv.2016.10.231

Gao M, Saide PE, Xin JY, Wang YS, Liu ZR, Wang YX, et al. Estimates of Health Impacts and Radiative Forcing in Winter Haze in Eastern China through Constraints of Surface PM2.5 Predictions. Environmental Science & Technology 2017b; 51: 2178-2185. https://doi.org/10.1021/acs.est.6b03745

Heese B, Baars H, Bohlmann S, Althausen D, Deng RR. Continuous vertical aerosol profiling with a multi-wavelength Raman polarization lidar over the Pearl River Delta, China. Atmospheric Chemistry and Physics 2017; 17: 6679-6691. https://doi.org/10.5194/acp-17-6679-2017

Hong QQ, Liu C, Chan KL, Hu QH, Xie ZQ, Liu HR, et al. Ship-based MAX-DOAS measurements of tropospheric NO2, SO2, and HCHO distribution along the Yangtze River. Atmospheric Chemistry and Physics 2018; 18: 5931-5951. https://doi.org/10.5194/acp-18-5931-2018

Hu M, Guo S, Peng JF, Wu ZJ. Insight into characteristics and sources of PM2.5 in the Beijing-Tianjin-Hebei region, China. National Science Review 2015; 2: 257-258. https://doi.org/10.1093/nsr/nwv003

Hua Y, Cheng Z, Wang SX, Jiang JK, Chen DR, Cai SY, et al. Characteristics and source apportionment of PM2.5 during a fall heavy haze episode in the Yangtze River Delta of China. Atmospheric Environment 2015; 123: 380-391. https://doi.org/10.1016/j.atmosenv.2015.03.046

Huang M, Crawford JH, Diskin GS, Santanello JA, Kumar SV, Pusede SE, et al. Modeling Regional Pollution Transport Events During KORUS-AQ: Progress and Challenges in Improving Representation of Land-Atmosphere Feedbacks. Journal of Geophysical Research-Atmospheres 2018a; 123: 10732-10756. https://doi.org/10.1029/2018jd028554

Huang X, Wang Z, Ding A. Impact of Aerosol-PBL Interaction on Haze Pollution: Multiyear Observational Evidences in North China. Geophysical Research Letters 2018b; 45: 8596-8603. https://doi.org/10.1029/2018gl079239

Huang X, Zhou LX, Ding AJ, Qi XM, Nie W, Wang MH, et al. Comprehensive modelling study on observed new particle formation at the SORPES station in Nanjing, China. Atmospheric Chemistry and Physics 2016; 16: 2477-2492. https://doi.org/10.5194/acp-16-2477-2016

Jiang ZQ, Liu ZQ, Wang TJ, Schwartz CS, Lin HC, Jiang F. Probing into the impact of 3DVAR assimilation of surface PM10 observations over China using process analysis. Journal of Geophysical Research-Atmospheres 2013; 118: 6738-6749. https://doi.org/10.1002/jgrd.50495

https://doi.org/10.5194/acp-2020-1273
Preprint. Discussion started: 8 January 2021

Klett JD. Stable Analytical Inversion Solution for Processing Lidar Returns. Applied Optics 1981; 20: 211-220. https://doi.org/10.1364/Ao.20.000211

Kumar M, Raju MP, Singh RK, Singh AK, Singh RS, Banerjee T. Wintertime characteristics of aerosols over middle Indo-Gangetic Plain: Vertical profile, transport and radiative forcing. Atmospheric Research 2017; 183: 268-282. https://doi.org/10.1016/j.atmosres.2016.09.012

Li J, Du HY, Wang ZF, Sun YL, Yang WY, Li JJ, et al. Rapid formation of a severe regional winter haze episode over a mega-city cluster on the North China Plain. Environmental Pollution 2017a; 223: 605-615. https://doi.org/10.1016/j.envpol.2017.01.063

Li X, Zhang Q, Zhang Y, Zhang L, Wang YX, Zhang QQ, et al. Attribution of PM2.5 exposure in Beijing-Tianjin-Hebei region to emissions: implication to control strategies. Science Bulletin 2017b; 62: 957-964. https://doi.org/10.1016/j.scib.2017.06.005

Li YR, Ye CX, Liu J, Zhu Y, Wang JX, Tan ZQ, et al. Observation of regional air pollutant transport between the megacity Beijing and the North China Plain. Atmospheric Chemistry and Physics 2016; 16: 14265-14283. https://doi.org/10.5194/acp-16-14265-2016

Li ZQ, Guo JP, Ding AJ, Liao H, Liu JJ, Sun YL, et al. Aerosol and boundary-layer interactions and impact on air quality. National Science Review 2017c; 4: 810-833. https://doi.org/10.1093/nsr/nwx117

Liu ZQ, Liu QH, Lin HC, Schwartz CS, Lee YH, Wang TJ. Three-dimensional variational assimilation of MODIS aerosol optical depth: Implementation and application to a dust storm over East Asia. Journal Of Geophysical Research-Atmospheres 2011; 116. https://doi.org/10.1029/2011jd016159

Lu LH, Liu WQ, Zhang TS, Lu YH, Dong YS, Chen ZY, et al. Two Data Inversion Algorithms of Aerosol Horizontal Distribution Detected by MPL and Error Analysis. Spectroscopy and Spectral Analysis 2015; 35: 1774-1778. https://doi.org/10.3964/j.issn.1000-0593(2015)07-1774-05

Lv L, Liu W, Zhang T, Chen Z, Dong Y, Fan G, et al. Observations of particle extinction, PM 2.5 mass concentration profile and flux in north China based on mobile lidar technique. Atmospheric Environment 2017a. https://doi.org/10.1016/j.atmosenv.2017.06.022

Lv LH, Liu WQ, Zhang TS, Chen ZY, Dong YS, Fan GQ, et al. Observations of particle extinction, PM2.5 mass concentration profile and flux in north China based on mobile lidar technique. Atmospheric Environment 2017b; 164: 360-369. https://doi.org/10.1016/j.atmosenv.2017.06.022

Ma CQ, Wang TJ, Mizzi AP, Anderson JL, Zhuang BL, Xie M, et al. Multiconstituent Data Assimilation With WRF-Chem/DART: Potential for Adjusting Anthropogenic Emissions and Improving Air Quality Forecasts Over Eastern China. Journal of Geophysical Research-Atmospheres 2019; 124: 7393-7412. https://doi.org/10.1029/2019jd030421

Ma CQ, Wang TJ, Zang ZL, Li ZJ. Comparisons of Three-Dimensional Variational Data Assimilation and Model Output Statistics in Improving Atmospheric Chemistry Forecasts. Advances in Atmospheric Sciences 2018; 35: 813-825. https://doi.org/10.1007/s00376-017-7179-y

Pagowski M, Liu Z, Grell GA, Hu M, Lin HC, Schwartz CS. Implementation of aerosol assimilation in Gridpoint Statistical Interpolation (v. 3.2) and WRF-Chem (v. 3.4.1). Geoscientific Model Development 2014; 7: 1621-1627. https://doi.org/10.5194/gmd-7-1621-2014

Pang JM, Liu ZQ, Wang XM, Bresch J, Ban JM, Cnen D, et al. Assimilating AOD retrievals from GOCI and VIIRS to forecast surface PM2.5 episodes over Eastern China.

https://doi.org/10.5194/acp-2020-1273
Preprint. Discussion started: 8 January 2021

Atmospheric Chemistry and Physics Discussions

Atmospheric Environment 2018; 179: 288-304. https://doi.org/10.1016/j.atmosenv.2018.02.011

Parrish DF, Derber JC. The National Meteorological Center's Spectral Statistical-Interpolation Analysis System. Monthly Weather Review 1992; 120: 1747-1763. https://doi.org/10.1175/1520-0493(1992)120<1747:Tnmcss>2.0.Co;2

Pokharel M, Guang J, Liu B, Kang S, Ma Y, Holben BN, et al. Aerosol Properties Over Tibetan Plateau From a Decade of AERONET Measurements: Baseline, Types, and Influencing Factors. Journal of Geophysical Research: Atmospheres 2019; 124: 13357-13374. https://doi.org/10.1029/2019jd031293

Saide PE, Carmichael GR, Liu Z, Schwartz CS, Lin HC, da Silva AM, et al. Aerosol optical depth assimilation for a size-resolved sectional model: impacts of observationally constrained, multi-wavelength and fine mode retrievals on regional scale analyses and forecasts. Atmospheric Chemistry And Physics 2013; 13: 10425-10444. https://doi.org/10.5194/acp-13-10425-2013

Saide PE, Kim J, Song CH, Choi M, Cheng YF, Carmichael GR. Assimilation of next generation geostationary aerosol optical depth retrievals to improve air quality simulations. Geophysical Research Letters 2014; 41: 9188-9196. https://doi.org/10.1002/2014GL062089

Schwartz CS, Liu ZQ, Lin HC, McKeen SA. Simultaneous three-dimensional variational assimilation of surface fine particulate matter and MODIS aerosol optical depth. Journal of Geophysical Research-Atmospheres 2012; 117. https://doi.org/10.1029/2011jd017383

Sheng ZZ, Che HZ, Chen QL, Xia XA, Liu D, Wang ZZ, et al. Aerosol vertical distribution and optical properties of different pollution events in Beijing in autumn 2017. Atmospheric Research 2019; 215: 193-207. https://doi.org/10.1016/j.atmosres.2018.08.029

Su H, Cheng Y, Poschl U. New Multiphase Chemical Processes Influencing Atmospheric Aerosols, Air Quality, and Climate in the Anthropocene. Acc Chem Res 2020. https://doi.org/10.1021/acs.accounts.0c00246

Sun J, Huang L, Liao H, Li J, Hu J. Impacts of Regional Transport on Particulate Matter Pollution in China: a Review of Methods and Results. Current Pollution Reports 2017; 3: 182-191. https://doi.org/10.1007/s40726-017-0065-5

Tao W, Su H, Zheng G, Wang J, Wei C, Liu L, et al. Aerosol pH and chemical regimes of sulfate formation in aerosol water during winter haze in the North China Plain. Atmos. Chem. Phys. Discuss. 2020; 2020: 1-31. https://doi.org/10.5194/acp-2020-177

Tao ZM, Wang ZZ, Yang SJ, Shan HH, Ma XM, Zhang H, et al. Profiling the PM2.5 mass concentration vertical distribution in the boundary layer. Atmospheric Measurement Techniques 2016; 9: 1369-1376. https://doi.org/10.5194/amt-9-1369-2016

Tian PF, Cao XJ, Zhang L, Sun NX, Sun L, Logan T, et al. Aerosol vertical distribution and optical properties over China from long-term satellite and ground-based remote sensing. Atmospheric Chemistry and Physics 2017; 17: 2509-2523. https://doi.org/10.5194/acp-17-2509-2017

Wang J, Zhang M, Bai X, Tan H, Li S, Liu J, et al. Large-scale transport of PM2.5 in the lower troposphere during winter cold surges in China. Sci Rep 2017; 7: 13238. https://doi.org/10.1038/s41598-017-13217-2

Wang LL, Liu JK, Gao ZQ, Li YB, Huang M, Fan SH, et al. Vertical observations of the atmospheric boundary layer structure over Beijing urban area during air pollution episodes. Atmospheric Chemistry and Physics 2019; 19: 6949-6967. https://doi.org/10.5194/acp-19-6949-2019

https://doi.org/10.5194/acp-2020-1273
Preprint. Discussion started: 8 January 2021

Atmospheric Chemistry and Physics Discussions

Wang LL, Liu ZR, Sun Y, Ji DS, Wang YS. Long-range transport and regional sources of PM2.5 in Beijing based on long-term observations from 2005 to 2010. Atmospheric Research 2015; 157: 37-48. https://doi.org/10.1016/j.atmosres.2014.12.003

Wang Y, Sartelet KN, Bocquet M, Chazette P. Assimilation of ground versus lidar observations for PM10 forecasting. Atmospheric Chemistry and Physics 2013; 13: 269-283. https://doi.org/10.5194/acp-13-269-2013

Xiang Y, Lv L, Chai W, Zhang T, Liu J, Liu W. Using Lidar technology to assess regional air pollution and improve estimates of PM2.5 transport in the North China Plain. Environmental Research Letters 2020; 15: 094071. https://doi.org/10.1088/1748-9326/ab9cfd

Xiang Y, Zhang TS, Liu JG, Lv LH, Dong YS, Chen ZY. Atmosphere boundary layer height and its effect on air pollutants in Beijing during winter heavy pollution. Atmospheric Research 2019; 215: 305-316. https://doi.org/10.1016/j.atmosres.2018.09.014

Xu JM, Chang LY, Qu YH, Yan FX, Wang FY, Fu QY. The meteorological modulation on PM2.5 interannual oscillation during 2013 to 2015 in Shanghai, China. Science Of the Total Environment 2016; 572: 1138-1149. https://doi.org/10.1016/j.scitotenv.2016.08.024

Yang X, Cheng S, Li J, Lang J, Wang G. Characterization of Chemical Composition in PM2.5 in Beijing before, during, and after a Large-Scale International Event. Aerosol and Air Quality Research 2017; 17: 896-907. https://doi.org/10.4209/aaqr.2016.07.0321

Yuan RM, Zhang XY, Liu H, Gui Y, Shao BH, Tao XP, et al. Aerosol vertical mass flux measurements during heavy aerosol pollution episodes at a rural site and an urban site in the Beijing area of the North China Plain. Atmospheric Chemistry and Physics 2019; 19: 12857-12874. https://doi.org/10.5194/acp-19-12857-2019

Yumimoto K, Uno I, Sugimoto N, Shimizu A, Liu Z, Winker DM. Adjoint inversion modeling of Asian dust emission using lidar observations. Atmospheric Chemistry and Physics 2008; 8: 2869-2884. https://doi.org/DOI 10.5194/acp-8-2869-2008

Zhang CX, Liu C, Chan KL, Hu QH, Liu HR, Li B, et al. First observation of tropospheric nitrogen dioxide from the Environmental Trace Gases Monitoring Instrument onboard the GaoFen-5 satellite. Light-Science & Applications 2020; 9. https://doi.org/10.1038/s41377-020-0306-z

Zhang CX, Liu C, Hu QH, Cai ZN, Su WJ, Xia CZ, et al. Satellite UV-Vis spectroscopy: implications for air quality trends and their driving forces in China during 2005-2017. Light-Science & Applications 2019a; 8. https://doi.org/10.1038/s41377-019-0210-6

Zhang H, Cheng S, Yao S, Wang X, Wang C. Insights into the temporal and spatial characteristics of PM2.5 transport flux across the district, city and region in the North China Plain. Atmospheric Environment 2019b; 218. https://doi.org/10.1016/j.atmosenv.2019.117010

Zhang H, Xie B, Zhao S-Y, Chen Q. PM2.5 and tropospheric O3 in China and an analysis of the impact of pollutant emission control. Advances in Climate Change Research 2014; 5: 136-141. https://doi.org/10.1016/j.accre.2014.11.005

Zhang Q, Zheng YX, Tong D, Shao M, Wang SX, Zhang YH, et al. Drivers of improved PM2.5 air quality in China from 2013 to 2017. Proceedings of the National Academy of Sciences of the United States of America 2019c; 116: 24463-24469. https://doi.org/10.1073/pnas.1907956116

Zhang Y, Zhang X, Wang LT, Zhang Q, Duan FK, He KB. Application of WRF/Chem over East Asia: Part I. Model evaluation and intercomparison with MM5/CMAQ. Atmospheric Environment 2016; 124: 285-300. https://doi.org/10.1016/j.atmosenv.2015.07.022

https://doi.org/10.5194/acp-2020-1273
Preprint. Discussion started: 8 January 2021

Atmospheric Chemistry and Physics Discussions

Zhang YH, Su H, Zhong LJ, Cheng YF, Zeng LM, Wang XS, et al. Regional ozone pollution and observation-based approach for analyzing ozone-precursor relationship during the PRIDE-PRD2004 campaign. Atmospheric Environment 2008; 42: 6203-6218. https://doi.org/10.1016/j.atmosenv.2008.05.002

Zhang YL, Cao F. Fine particulate matter (PM2.5) in China at a city level. Scientific Reports 2015; 5. https://doi.org/10.1038/srep14884

Zhang YX, Yuan Q, Huang D, Kong SF, Zhang J, Wang XF, et al. Direct Observations of Fine Primary Particles From Residential Coal Burning: Insights Into Their Morphology, Composition, and Hygroscopicity. Journal of Geophysical Research-Atmospheres 2018; 123: 12964-12979. https://doi.org/10.1029/2018jd028988

Zhao D, Liu G, Xin J, Quan J, Wang Y, Wang X, et al. Haze pollution under a high atmospheric oxidization capacity in summer in Beijing: insights into formation mechanism of atmospheric physicochemical processes. Atmos. Chem. Phys. 2020; 20: 4575-4592. https://doi.org/10.5194/acp-20-4575-2020

Zheng GJ, Duan FK, Su H, Ma YL, Cheng Y, Zheng B, et al. Exploring the severe winter haze in Beijing: the impact of synoptic weather, regional transport and heterogeneous reactions. Atmospheric Chemistry and Physics 2015; 15: 2969-2983. https://doi.org/10.5194/acp-15-2969-2015

Zheng M, Yan CQ, Wang SX, He KB, Zhang YH. Understanding PM2.5 sources in China: challenges and perspectives. National Science Review 2017; 4: 801-803. https://doi.org/10.1093/nsr/nwx129

Zheng Y, Che HZ, Xia XG, Wang YQ, Wang H, Wu YF, et al. Five-year observation of aerosol optical properties and its radiative effects to planetary boundary layer during air pollution episodes in North China: Intercomparison of a plain site and a mountainous site in Beijing. Science of the Total Environment 2019; 674: 140-158. https://doi.org/10.1016/j.scitotenv.2019.03.418

Zhong JT, Zhang XY, Wang YQ, Sun JY, Zhang YM, Wang JZ, et al. Relative Contributions of Boundary-Layer Meteorological Factors to the Explosive Growth of PM2.5 during the Red-Alert Heavy Pollution Episodes in Beijing in December 2016. Journal of Meteorological Research 2017; 31: 809-819. https://doi.org/10.1007/s13351-017-7088-0

Zhou YD, Zhao Y, Mao P, Zhang Q, Zhang J, Qiu LP, et al. Development of a high-resolution emission inventory and its evaluation and application through air quality modeling for Jiangsu Province, China. Atmospheric Chemistry and Physics 2017; 17: 211-233. https://doi.org/10.5194/acp-17-211-2017